Hellinger Kernel-based Distance and Local Image Region Descriptors for Sky Region Detection from Fisheye Images

Y. El Merabet[1], Y. Ruichek[2], S. Ghaffarian[3], Z. Samir[1], T. Boujiha[1], R. Touahni[1], R. Messoussi[1] and A. Sbihi[4]

[1]*Laboratoire LASTID, Département de Physique, Faculté des Sciences, Université Ibn Tofail, B.P 133, 14000, Kénitra, Morocco*

[2]*Laboratoire IRTES-SeT, Université de Technologie de Belfort-Montbéliard, 13 rue Ernest Thierry-Mieg, 90010, Belfort, France*

[3]*Faculty of Geo-Information Science and Earth Observation (ITC), University of Twente, Enschede, 7500 AE, The Netherlands*

[4]*Laboratoire LABTIC, ENSA, Université Abdelmalek Essadi, Route Ziaten, km 10, BP 1818 Tanger, Morocco*

Keywords: GNSS, Region Classification, Image Segmentation, Fisheye, Color Invariance, Hellinger Kernel, Local Image Region Descriptors.

Abstract: Characterizing GNSS signals reception environment using fisheye camera oriented to the sky is one of the relevant approaches which have been proposed to compensate the lack of performance of GNSS occurring when operating in constrained environments (dense urbain areas). This solution consists, after classification of acquired images into two regions (sky and not-sky), in identifying satellites as line-of-sight (LOS) satellites or non-line-of-sight (NLOS) satellites by repositioning the satellites in the classified images. This paper proposes a region-based image classification method through local image region descriptors and Hellinger kernel-based distance. The objective is to try to improve results obtained previously by a state of the art method. The proposed approach starts by simplifying the acquired image with a suitable couple of colorimetric invariant and exponential transform. After that, a segmentation step is performed in order to extract from the simplified image regions of interest using Statistical Region Merging method. The next step consists of characterizing the obtained regions with local RGB color and a number of local color texture descriptors using image quantization. Finally, the characterized regions are classified into sky and non sky regions by using supervised $\mathcal{MSRC}$ (Maximal Similarity Based Region Classification) method through Hellinger kernel-based distance. Extensive experiments have been performed to prove the effectiveness of the proposed approach.

1 INTRODUCTION

GNSS systems (Global Navigation Satellites Systems), such as COMPASS, GLONASS, GPS and European GALILEO have the potential to advance the development of intelligent transport systems (ITSs) and associated services. They contribute widely to localization and navigation systems and provide useful information that can for example be exploited in a meaningful way in the field of transport market such as fleet management, monitoring of containers, etc. One of the main drawbacks of GNSSs systems in constrained environments such as urban zones is that signals may arrive at the receiver antenna only in non-line-of-sight (NLOS) conditions. Indeed, even if most of them give satisfying accuracy in terms of position of localization, they cannot avoid propagation problems caused by multi-path phenomena (cf. Figure 1) of GNSS signals. This can be explained by the fact that in dense environments, like city centers, signals can be shadowed (signal received after reflections without any direct ray), blocked (no signal received) and directly received. Consequently, the evaluation of estimated position reliability remains challenging in presence of these constraints. For applications like containers monitoring, flot management, etc., not requiring high availability, integrity and accuracy of the positioning system, this drawback is only a marginal problem. But this constitutes a real challenge for specific applications dealing with liability issues (toll, insurance, etc.) as well as safety-related applications (automatic guidance or control), requiring more stringent performances. Several solutions have been proposed in the literature in order to enhance localization

El Merabet Y., Ruichek Y., Ghaffarian S., Samir Z., Boujiha T., Touahni R., Messoussi R. and Sbihi A.
Hellinger Kernel-based Distance and Local Image Region Descriptors for Sky Region Detection from Fisheye Images.
DOI: 10.5220/0006092404190427
In *Proceedings of the 12th International Joint Conference on Computer Vision, Imaging and Computer Graphics Theory and Applications (VISIGRAPP 2017)*, pages 419-427
ISBN: 978-989-758-225-7

accuracy. One can cite those increasing the system complexity like multi-sensor-based approaches that consist to add other sensors (odometer, Inertial Measurement Unit, etc.) to compensate the lack of performance of GNSS (Wang and Gao, 2007; Lentmaier et al., 2008). Using complementarity between localization systems and computer vision to characterize the environment of reception of satellites is another workaround that is recently proposed (Marais et al., 2013). The idea consists in analyzing the structure of the environment traveled by a vehicle using a single camera delivering visible range to overcome problems such as time computation, lack of precision of 3D models, etc. The approach relies, at each acquisition of a fisheye image using a wide-angle camera (fisheye camera with a large field of view of 180°) mounted near to a GPS receiver on the roof of the vehicle and oriented to the sky, on sequentially applying of two major steps: 1/ image processing and 2/ repositioning. The objective of the first step is to automatically detect sky region from the acquired image. For that, a geodesic reconstruction based technique with an optimal contrast parameter is used in order to simplify the fisheye image. Then, the pixels of the obtained simplified image are classified into two classes (sky and not-sky) using image clustering. A set of unsupervised (Km local, Fuzzy Cmeans, Fisher and Statistical region Merging) and supervised (Bayes, K-Nearest Neighbor and Support Vector Machine) clustering algorithms have been tested and compared. In the second step, the satellites are repositioned in classified image to identify GNSS signals with direct path (resp. blocked/reflected signals) i.e. located in sky region of the image (resp. located in not-sky region). More details of this repositioning step can be found in (Marais et al., 2013). Obviously, the reliability of the proposed procedure depends greatly on the results of image processing step, i.e. the classification results. In this paper, our challenge consists in making this step more effective in terms of image classification results. Figure 2 illustrates the flowshart of the image processing-based method for localization. The method is composed of two major steps : image processing and localization. Our contribution is concerned with the image processing part. The method we propose is composed of several substeps: 1/ image simplification, 2/ image segmentation, 3/ region features extraction and 4/ region classification.

The paper is organized as follows: Section II presents the fisheye image simplification step of the proposed procedure. Section III introduces briefly the Statistical Region Merging algorithm used to obtain the preliminary fisheye image segmentation. In section IV, we introduce the implemented local color RGB, color local texture and color hybrid histograms as local image region descriptors. Section V presents the proposed $\mathcal{MSRC}$ algorithm. Experimental results and a comparison with the method of (Marais et al., 2013) are shown in Section VI. Conclusions are derived in Section VII.

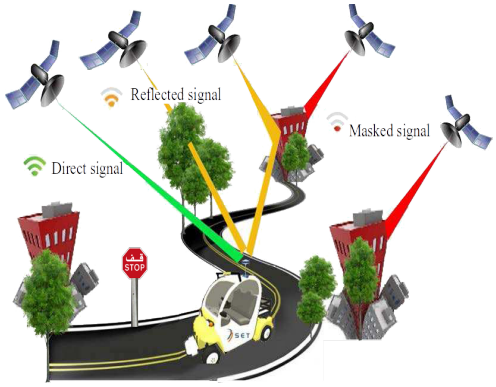

Figure 1: Illustration of the multipath phenomenon in urban areas.

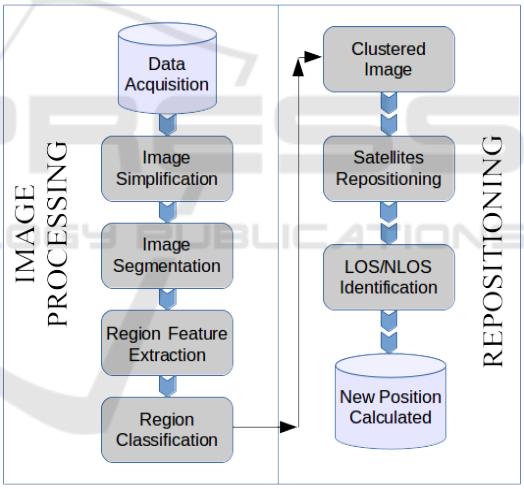

Figure 2: Flowshart of the image processing-based method for localization.

2 FISHEYE IMAGE SIMPLIFICATION

Image simplification is a very important basic ingredient of a lot of practical image-based applications. This useful basic pre-processing step permits to reduce content information of an image by suppressing undesired details such as noise. In this work, in order to simplify the acquired fisheye image, we opted to use color invariance and exponential transform. The sequential use of these two tools permits us to consid-

erably reduce the over-segmentation problem and to reach a more precise segmentation that is faithful to the desired real objects.

2.1 Color Invariance

In mobility with a mobile platform, as is the case of our application, several factors such as the surface reflectance, illuminant color, lighting geometry, response of the sensor, etc. (see Figure 4), may affect the quality of the acquired images. Consequently, attempting to segment the acquired image without any pre-processing step, leads to a strongly over-segmented image caused by insignificant structures or noise. To overcome this shortcoming and therefore to achieve satisfactory segmentation results (extract sky regions with high accuracy), the trend towards obtaining invariant signatures seems to be the best way forward (El merabet et al., 2011; El merabet et al., 2014; El merabet et al., 2015). Indeed, we propose to transform the input fisheye image using a colorimetric invariant in order to obtain a color-invariant fisheye image whatever the illumination conditions and artifacts present in the acquired images (noise and unimportant fine-scale details). In this work, we have used Affine Normalization (AN) expressed below (Fusiello et al., 1999). As it will be shown in section 6.2, tests have validated the interest in using this colorimetric invariant in the simplification process.

$$\begin{cases} f^R(p) = \frac{I^R(p)-\mu(I^R(p))}{std(I^R(p))} \\ f^G(p) = \frac{I^G(p)-\mu(I^G(p))}{std(I^G(p))} \\ f^B(p) = \frac{I^B(p)-\mu(I^B(p))}{std(I^B(p))} \end{cases} \quad (1)$$

where $I^K(p)$ is the pixel value at position p in the color component K={R, G, B}, $\mu(I^K(p))$ and $std(I^K(p))$ are, respectively, the mean value and standard deviation calculated in a window of interest $\mathcal{W}$ centered on the pixel p. This normalization ensures the invariance under affine changes of illumination that is achieved by independently normalizing each channel to have zero mean and unit variance.

2.2 Exponential Transform (ET)

Besides obtaining invariant signatures, image enhancement is another effective technique allowing to improve the robustness of image simplification process. The principal objective of this second component of image simplification module is to modify attributes of an image to make it more suitable for the considered application. In this paper, in order to efficiently improve segmentation quality results of fisheye images, we have opted to use the exponential transform (ET). ET permits to approximate the exponential correction factor of grayscale images which maximizes the contrast of the images in the class of exponential intensity mapping functions. Mathematically, ET is given by (cf. Eq. 2):

$$\begin{cases} I'_{ij} = exp(\chi/\xi) - 1 + I'_{min} \\ \chi = I_{ij} - I_{min} \\ \xi = (I_{max} - I_{min})/(log(I'_{max} - I'_{min} + 1)) \end{cases} \quad (2)$$

where I_{ij} is the intensity of the pixel at position (i, j), I_{max} and I_{min} are the highest and lowest intensities of the image I, respectively and ξ is a normalization factor for stretching output values between the new lowest I'_{min} and highest I'_{max} intensities of the resultant image I'.

3 PRELIMINARY FISHEYE IMAGE SEGMENTATION

As indicated previously, the second step of our approach relies on image segmentation in order to segment the simplified images into homogeneous regions with the same properties. Obviously, the quality of the classification results which are the output of the proposed region based classification procedure is strongly dependent on the segmentation results. In this paper, in order to obtain a preliminary fisheye image segmentation, we have used SRM (Statistical Region Merging) algorithm (Nock and Nielsen, 2004) that seems to be more adapted when considering the objectives of our application. Indeed, using this method, we can correctly extracts all significant regions where the boundaries hypothesized coincide with the significant segment boundaries in the simplified fisheye images. SRM algorithm presents several advantages : 1/ it dispenses dynamical maintenance of region adjacency graph (RAG); 2/ it allows defining a hierarchy of partitions; 3/ it runs in linear-time by using bucket sorting algorithm while transversing the RAG and 4/ it not only considers spectral, shape and scale information, but also has the ability to cope with significant noise corruption and handle occlusions.

4 REGION FEATURES

This stage of our approach consists in characterizing the segmented regions, obtained by using SRM algorithm, with suitable descriptors to identify the regions corresponding to the sky in fisheye images. The extraction of these descriptors, used as inputs to the proposed region based image classification, permits to

provide a global representation of a region that is a higher level than that of the raw image pixels allowing thus, to discriminate robustly between the different regions in the treated images. The descriptors we have choosen for the tests are explained below.

4.1 Local Color RGB Histograms

In spite of the fact that RGB color histogram is very simple, easiest feature to implement and low level method, it still being relevant for color based image classification. In the present study, RGB color histogram is implemented as follows: each RGB color channel is first uniformly quantized into l levels, after that, the color histogram of each segmented region is produced in the feature space of $z = l \times l \times l$ bins. Let I be an image containing N pixels quantized in z=16×16×16=4096 color bins, the RGB color histogram of a segmented region $\mathcal{R}$ is represented as

$$\mathcal{H}^{RGB}(\mathcal{R}) = [\mathcal{H}^1_{\mathcal{R}}, \mathcal{H}^2_{\mathcal{R}}, ..., \mathcal{H}^z_{\mathcal{R}}] \quad (3)$$

where

$$\mathcal{H}^i_{\mathcal{R}} = \sqrt{(\frac{\sum_{j=1}^{N} p_{i|j}}{\tau})}; \mathrm{j} \in \mathcal{R} \text{ and } 0 \leqslant \mathrm{i} \leqslant \mathrm{z}. \quad (4)$$

$\mathcal{H}^i_{\mathcal{R}}$ is the ith normalized histogram bin and τ=card($\mathcal{R}$) is the number of pixels in the region $\mathcal{R}$. $p_{i|j}$ is the conditional probability of the selected jth pixel belonging to the ith color bin. It is expressed as follows:

$$p_{i|j} = \begin{cases} 1, \text{if the } j\text{th pixel is quantized into the } i\text{th color bin} \\ 0, \text{otherwise.} \end{cases} \quad (5)$$

4.2 Color Local Texture Histograms

Texture analysis plays an important role in many disciplines and related applications: defect detection and food inspection, surface grading, computer assisted diagnosis, remote sensing, etc. (Dornaika et al., 2016), due to its potential in extracting prominent features with very high discriminating power.

It ressorts from the literature that the most proposed texture descriptors are developed for gray level images. Exploiting color aspects of textured images, which is one of the objectives of this work, has unfortunately received much less attention (Chao et al., 2013; Choi et al., 2012). Generally, the choice of suitable texture descriptor is closely related to the particularities of objects to be extracted from the image. In this work, we propose to investigate the impact of several well-known texture descriptors on the outcome of the proposed region based fisheye image classification. A set of 10 texture features calculated for each region of the segmented fisheye image are used and tested (cf. Table 1). In order to incorporate color information, these texture descriptors are extended to RGB color space producing thus 10 color local texture histograms ($\mathcal{H}^{LBP}$, $\mathcal{H}^{CSLBP}$, $\mathcal{H}^{LDP}$, $\mathcal{H}^{ILTP}$, etc.). The method consists in calculating the unichrome texture feature independently over different channels in RGB color space, concatenate them to get a descriptor color image (for example the LBP color image in Figure 3) and then the color local texture histogram is calculated for each region of the segmented image by following the same steps as for RGB color histograms, as shown in Figure 3.

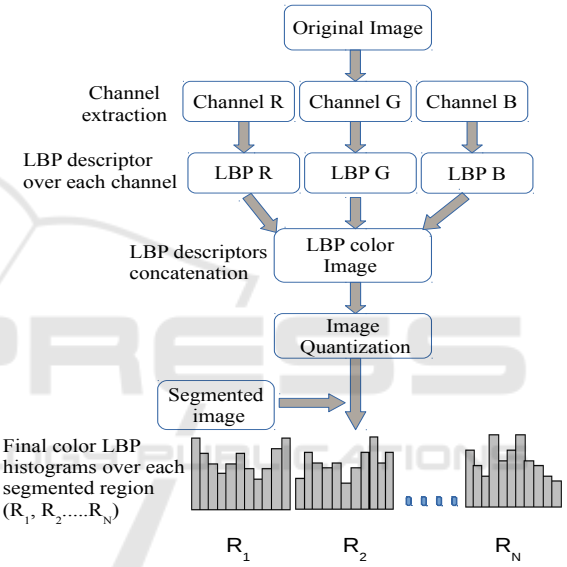

Figure 3: Calculation of color LBP histogram over each region of the segmented image.

4.3 Local Hybrid Histograms

In order to build local hybrid histograms, we propose to concatenate the feature vectors provided by different descriptors. Given two local color histograms $\mathcal{H}(\mathcal{R}) = [\mathcal{H}^1_{\mathcal{R}}, \mathcal{H}^2_{\mathcal{R}}, ..., \mathcal{H}^z_{\mathcal{R}}]$ and $\mathcal{H}'(\mathcal{R}) = [\mathcal{H}^{1'}_{\mathcal{R}}, \mathcal{H}^{2'}_{\mathcal{R}}, ..., \mathcal{H}^{z'}_{\mathcal{R}}]$ of a region $\mathcal{R}$, the corresponding local hybrid color histogram is mathematically represented as:

$$\begin{aligned} \mathcal{H}^{hyb}(\mathcal{R}) &= [\mathcal{H}_{\mathcal{R}}\ \mathcal{H}'_{\mathcal{R}}] \\ &= [\mathcal{H}^1_{\mathcal{R}}, \mathcal{H}^2_{\mathcal{R}}, .., \mathcal{H}^z_{\mathcal{R}}, \mathcal{H}^{1'}_{\mathcal{R}}, \mathcal{H}^{2'}_{\mathcal{R}}, .., \mathcal{H}^{z'}_{\mathcal{R}}] \end{aligned} \quad (6)$$

where $\mathcal{H}^i_{\mathcal{R}}$ is the ith histogram bins and the dimension of the obtained $\mathcal{H}^{hyb}(\mathcal{R})$ will be (2 × z) sized; z=16^3=4096.

Table 1: Texture descriptors extracted and used in this work.

Descriptors	Acronym	Ref.
Local binary patterns	LBP	(Ojala et al., 1996)
Orthogonal combination of local binary pattern	OCLBP	(Chao et al., 2013)
Local quinary patterns	LQP	(Nanni et al., 2010b)
Local ternary patterns	LTP	(Tan and Triggs, 2007)
Improved local ternary patterns	ILTP	(Nanni et al., 2010a)
Center-symmetric local binary patterns	CS-LBP	(Heikkilä et al., 2006)
3D Local binary patterns	3DLBP	(Huang et al., 2006)
Local derivative pattern	LDP	(Zhang et al., 2010)
Local phase quantization	LPQ	(Ojansivu et al., 2008)
Sum and difference histograms	SDH	(Unser, 1986)

In the present work, each one of the proposed color local texture histograms is concatenated with the color RGB histogram leading to 10 hybrid color texture histograms ($\mathcal{H}_{LBP}^{RGB}$, $\mathcal{H}_{ILTP}^{RGB}$, $\mathcal{H}_{OCLBP}^{RGB}$, $\mathcal{H}_{LPQ}^{RGB}$, etc.). While this can enrich the discrimination capacity of the resulting descriptor, it has the disadvantage that the dimensionality of the resulting feature vector could be very high, increasing thus the computation time.

5 MAXIMAL SIMILARITY BASED REGION CLASSIFICATION

Since the segmented regions $\mathcal{M}_{\mathbf{SRM}}$, obtained via SRM algorithm, are now characterized with the descriptors introduced previously, our challenge is to classify them into sky and non-sky regions. For this purpose, we need to calculate similarity between the characterized regions ($\mathcal{R} \in \mathcal{M}_{\mathbf{SRM}}$) and those of two learning databases $\mathcal{B}_{\mathbf{obj}}$ and $\mathcal{B}_{\mathbf{back}}$ that are constructed respectively with m distinctive textures of sky regions and n distinctive textures of non-sky regions such as building, road, tree, etc. We have then to define a similarity measure $\Psi(\mathcal{R},\mathcal{Q})$ allowing to calculate similarity between two regions $\mathcal{R}$ and $\mathcal{Q}$ basing on their descriptors. Given two image region features f_1 and f_2, $\Psi(f_1,f_2)$ considers these image region features as points in the vector space and calculate close degree of two points. There are several well-known goodness-of-fit statistical metrics in the literature. One can cite second type distance (Stricker and Orengo, 1995), log-likelihood ratio statistic (Fukunaga, 1990), Minkowski measure, histogram intersection method (Swain and Ballard, 2002), Hellinger distance (Kailath, 1967; Ninga et al., 2010), etc. Let $\mathcal{H}_{\mathcal{R}}^{i}$ be the normalized histogram of a region $\mathcal{R}$, the superscript i represents its i^{th} element. $z = l \times l \times l = 4096$ represents the feature space. In this study, we have used Hellinger kernel (also known as Bhattacharyya coefficient given by Eq. 7), which represents the cosine of angle between the unit vectors representing the two regions to be compared:

$$(\sqrt{\mathcal{H}_{\mathcal{R}}^{1}}, ..., \sqrt{\mathcal{H}_{\mathcal{R}}^{z}})^T$$

and

$$(\sqrt{\mathcal{H}_{\mathcal{Q}}^{1}}, ..., \sqrt{\mathcal{H}_{\mathcal{Q}}^{z}})^T$$

The higher the Hellinger distance $\Psi(\mathcal{R},\mathcal{Q})$ between regions $\mathcal{R}$ and $\mathcal{Q}$ is, the higher the similarity between them is. That is to say that the angle between the two histogram vectors is very small involving that their histograms are very similar. Certainly, two similar histograms do not necessarily involve that the two corresponding regions are perceptually similar. Nevertheless, coupled with the proposed $\mathcal{MSRC}$ algorithm summarized in algorithm 1, Hellinger kernel based similarity works well in the proposed approach.

$$\Psi(\mathcal{R},\mathcal{Q}) = \sum_{i=1}^{z} \sqrt{\mathcal{H}_{\mathcal{R}}^{i}.\mathcal{H}_{\mathcal{Q}}^{i}} \qquad (7)$$

In our implementation, the main assumption of the proposed $\mathcal{MSRC}$ algorithm is that it assigns an unknown region R to a class C_n, if the average of the K first high similarity measures calculated between the region R and the regions of the learning database corresponding to the class C_n is maximal, i.e,

$$C^*(\mathcal{R}) = \arg\max_{C_n \in C} \frac{1}{K} \sum_{i=1}^{K} \Psi(\mathcal{R},\mathcal{Q}_i),\ \mathcal{Q}_i \in B_n \qquad (8)$$

where $B_1, B_2, ..., B_j$ are the learning databases corresponding to the classes $C_1, C_2, ..., C_j$, $\mathcal{R}$ is a query, and Ψ is the similarity measure.

6 RESULTS AND DISCUSSION

To evaluate and shown the effectiveness of the proposed $\mathcal{MSRC}$ method, the RGB color and the pro-

Algorithm 1: Maximal similarity based region classification.

Require: $I \leftarrow$ The set $\mathcal{M}_{\mathbf{SRM}}$ of segmented regions (after simplification of the input image using AN/ET conjointly).
$\mathcal{B}_{\mathbf{obj}} \leftarrow$ learning database of sky regions.
$\mathcal{B}_{\mathbf{back}} \leftarrow$ learning database of non sky regions (building, road, tree, etc.).

1: Calculate the local image region descriptor for all regions of $\mathcal{M}_{\mathbf{SRM}}$ and for those composing $\mathcal{B}_{\mathbf{obj}}$ and $\mathcal{B}_{\mathbf{back}}$.
2: **for** each candidate region $\mathcal{R} \in \mathcal{M}_{\mathbf{SRM}}$ **do**
3: Calculate $V^{R}_{obj} = \{\Psi(\mathcal{R}, Q_i); (Q_i)_{i=1..m} \in \mathcal{B}_{\mathbf{obj}}\}$, the similarity vector between $\mathcal{R}$ and $\mathcal{B}_{\mathbf{obj}}$. $\Psi(\mathcal{R}, Q_i)$ is the similarity between $\mathcal{R}$ and the region $Q_i \in \mathcal{B}_{\mathbf{obj}}$.
4: Calculate $V^{\mathcal{R}}_{back} = \{\Psi(\mathcal{R}, Q_j); (Q_j)_{j=1..n} \in \mathcal{B}_{\mathbf{back}}\}$, the similarity vector between $\mathcal{R}$ and $\mathcal{B}_{\mathbf{back}}$. $\Psi(\mathcal{R}, Q_j)$ is the similarity between $\mathcal{R}$ and the region $Q_j \in \mathcal{B}_{\mathbf{back}}$.
5: Get the order of $V^{\mathcal{R}}_{obj}$ and $V^{\mathcal{R}}_{back}$ by decreasing sorting;
6: Calculate $\mu^{\mathcal{R}}_{obj} = \frac{\sum_{i=1}^{K} \Psi(\mathcal{R}, Q_i)}{K}$, $K \leq m$, the mean of the K first elements of $V^{\mathcal{R}}_{obj}$.
7: Calculate $\mu^{\mathcal{R}}_{back} = \frac{\sum_{j=1}^{K} \Psi(\mathcal{R}, Q_j)}{K}$, $K \leq n$, the mean of the K first elements of $V^{\mathcal{R}}_{back}$.
8: **if** $(\mu^{\mathcal{R}}_{obj} \geq \mu^{\mathcal{R}}_{back})$ **then**
9: The region $\mathcal{R}$ has the maximal similarity with $\mathcal{B}_{\mathbf{obj}}$, it is then classified as a part of sky regions.
10: **else**
11: The region $\mathcal{R}$ has the maximal similarity with $\mathcal{B}_{\mathbf{back}}$, it is then classified as a part of background.
12: **end if**
13: **end for**
14: **return** The final segmentation map.

posed groups of color local texture and local hybrid image region descriptors for classification of regions extracted from fisheye images into two class (sky or non sky regions), several tests were carried out. As pointed out in the introduction, the main objective of this work consists in improving the results presented in (Marais et al., 2013). For that, a comparison step was also performed to show the improvement that our method provides.

6.1 Dataset

The image database acquired in the framework of the CAPLOC project (Marais et al., 2013), was used to validate the proposed sky detection approach from fisheye images. It has heterogeneous data and varying complex scenarios (overexposure, brightness changes, vegetation abundance, urban canyon, etc.). The image database contains 150 fisheye images exhibiting the mentioned various complex situations. Figure 4 Illustrates Six images of the database.

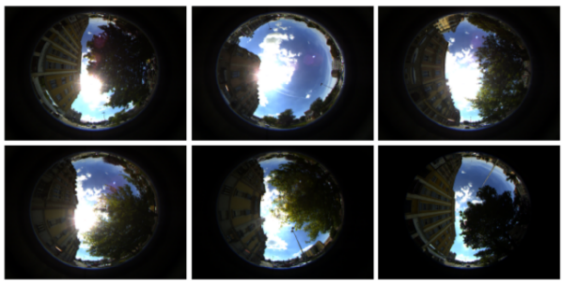

Figure 4: Six images of the database (acquired in the framework of the CAPLOC project).

6.2 Impact of the Couple AN/ET

As indicated in Section 2, the acquired fisheye image is firstly simplified using the couple of AN/ET where the objective is to limit illumination changes and thus reduce over-segmentation problem.

Table 2 highlights the ability of the couple AN/ET to reduce the number of segmented regions. It appears from this Table that when using Affine Normalization and the Exponential Transform conjointly, the number of regions is considerably reduced. Indeed, the use of this couple leads to a number of segmented regions greatly reduced (in average 10.43 regions per image) in comparison with that obtained without any simplification step. The reduction rate is 73.46%, i.e. the couple of AN/ET permits to eliminate (38.08-10.43)*150 images=4147.5 undesirable regions. In addition, the couple AN/ET provides good classification results where the produced classified images are most close to the corresponding ground truth (judged by the evaluation results given in Table 2). Indeed, the couple AN/ET allows obtaining 99.17% as a value for accuracy measure Vs 98.98% Vs 99.02% Vs 99.00% using AN without ET, RGB/ET and RGB without ET respectively.

6.3 $\mathcal{MSRC}$ and Descriptors Performance

In this section, we study the ability of the proposed $\mathcal{MSRC}$ method and the proposed groups of local image region descriptors to classify all regions of the segmented image into sky and non sky class.

Table 2: Average number of segmented regions per image and performance of the $\mathcal{MSRC}$ method using OCLBP as local image region descriptor.

	RGB	RGB/ET	AN	AN/ET
Number of regions	38.08	12.20	11.23	10.43
Accuracy (%)	99.00	99.02	98.98	99.17

In Table 3, we report the obtained experimental results according to the local color RGB, color local texture and color hybrid histograms used. The analysis of the accuracy measure leads us to highlight the influence of the use of hybrid descriptors. Indeed, when used in a hybrid form with RGB color histogram, all tested color local texture histograms give good results as they permit to increase the classification rate. However, it is worthy to notice that the $RGB \cup LBP$ and $RGB \cup ILTP$ descriptors are the most promising because they give the maximum classification rates compared to the other tested descriptors.

6.4 Comparative Evaluation and Discussion

As pointed out in Section 1, the main aim of this study is to improve the performance of the method introduced within the CAPLOC project (Marais et al., 2013). In this framework, the proposed approach mainly consists in classifying the acquired fisheye images (after a geodesic reconstruction based simplification) into sky and non-sky class. In this work, the authors have compared the performance of different well known clustering algorithms including unsupervised (Fisher, KMlocal, Fuzzy-Cmeans, SRM) and supervised (Bayes, KNN, SVM) classifiers. More details related to this work can be found in (Marais et al., 2013). This section is intended to compare our proposed approach with the framework of (Marais et al., 2013) used with all these clustering algorithms.

Figure 5 highlights the recognition accuracy obtained for each tested method. It can be seen that our approach shows higher performance than the method in (Marais et al., 2013) used with the tested popular classifiers. Indeed, the proposed method permits to reach 99.24% as a value for accuracy measure vs 97,71% with Fisher vs 97.67% with KNN, etc. This shows that our method allows to increase the accuracy with 1,53%.

We support these results by the illustration of Figure 6 that shows some examples of visual comparison of the region classification results. It appears from this visual analysis that the proposed method demonstrates excellent precision in terms of sky boundary extraction. In fact, for all of the images in the first row of Figure 6, the produced sky extraction results agree most closely with the corresponding ground truth. Note that the majority of the sky regions are detected with good boundary delineation whereas the method introduced in (Marais et al., 2013) leads to many false positives on buildings and vegetation areas and false negatives within sky area accompanied by a loss of several parts of sky.

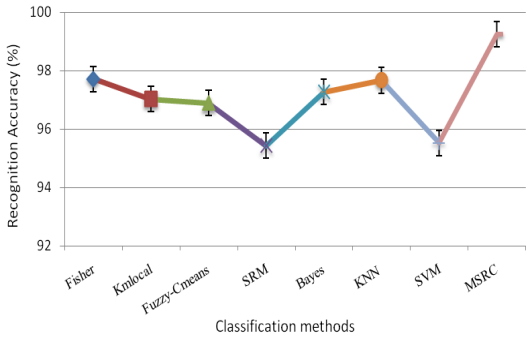

Figure 5: Classification results according to the method of (Marais et al., 2013) used with the tested popular classifiers and according to our proposed method.

7 CONCLUSION

The paper introduced a complete processing chain for horizon line detection from fisheye images, in the framework of enhancing GNSS based localization. The proposed method relies on a region based classification method using Hellinger kernel-based distance and a number of color, texture and hybrid image region descriptors. As a first step, we proposed to simplify the input images using Affine Normalization coupled with Exponential Transform in order to limit illumination changes (shadows, brightness, etc.) affecting the acquired fisheye images. Then, we have introduced several new local color descriptors for image region description based on texture features in order to characterize the regions obtained with the SRM algorithm. RGB color, a number of 10 color local texture and 10 local hybrid histograms have been introduced. As a final step, a Maximal Similarity Based Region Classification using Hellinger kernel-based distance has been proposed in order to identify candidate regions corresponding to targeted objects (sky regions in our case). The proposed approach was tested on image database containing 150 fisheye images allowing to obtain satisfying results with higher performance than that obtained with the method of (Marais et al., 2013) tested with several unsupervised (KMlocal, Fisher, fuzzy C-means and SRM) and supervised (Bayes, KNN and SVM) classifiers.

Table 3: Classification results according to the local color RGB histogram, color local texture and color hybrid histograms used.

Descriptors	Accuracy (%)	Hybrid Descriptors	Accuracy (%)
RGB	99.13	-	-
LBP	98.43	RGB ∪ LBP	99.24
CSLBP	96.92	RGB ∪ CSLBP	97.97
LPQ	93.42	RGB ∪ LPQ	99.18
3DLBP	93.33	RGB ∪ 3DLBP	97.97
LQP	96.34	RGB ∪ LQP	99.18
SDH	99.07	RGB ∪ SDH	99.13
LDP	96.11	RGB ∪ LDP	98.23
OCLBP	99.17	RGB ∪ OCLBP	99.22
LTP	97.29	RGB ∪ LTP	97.27
ILTP	97.81	RGB ∪ ILTP	99.24

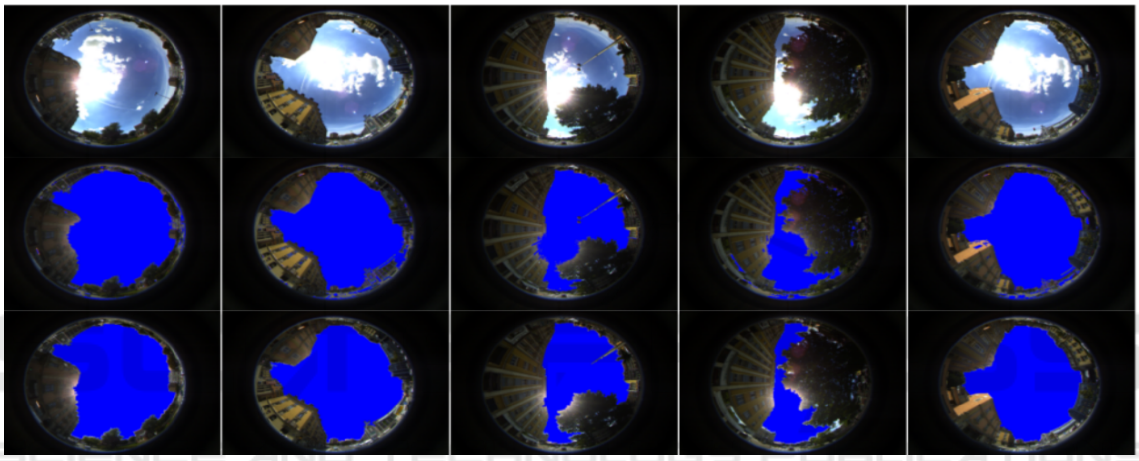

Figure 6: Visual comparison of region classification results. acquired images (first row); classified image into two classes (sky and non-sky) obtained by the best classifier defained in (Marais et al., 2013) (second row) and classification result obtained by the proposed $\mathcal{MSRC}$ approach (third row).

In future works, we envisage to extend the proposed approach to other data sets related to applications dealing with automatic objects recognition.

REFERENCES

Chao, Z., Charles, E., and Liming, C. (2013). Image region description using orthogonal combination of local binary patterns enhanced with color information. *Pattern Recognition*, 46:1949–1963.

Choi, J., Ro, Y., and Plataniotis, K. (2012). Color local texture features for color face recognition. *IEEE Trans. Image Proces*, 21(3):1366–1380.

Dornaika, F., Moujahid, A., El merabet, Y., and Ruichek, Y. (2016). Building detection from orthophotos using a machine learning approach: An empirical study on image segmentation and descriptors. *Expert Syst Appl*, 58:130–142.

El merabet, Y., Meurie, C., Ruichek, Y., Sbihi, A., and Touahni, R. (2011). Orthophotoplan segmentation and colorimetric invariants for roof detection. In *International Conference on Image Analysis and Processing, Springer Berlin Heidelberg*, pages 394–403.

El merabet, Y., Meurie, C., Ruichek, Y., Sbihi, A., and Touahni, R. (2014). Segmentation d'images aériennes par coopération lpe-régions et lpe-contours. application à la caractérisation de toitures. *Revue Francaise de Photogrammetrie et de Teledetection*, (206):9–44.

El merabet, Y., Meurie, C., Ruichek, Y., Sbihi, A., and Touahni, R. (2015). Building roof segmentation from aerial images using a line and region-based watershed segmentation technique. *Sensors*, 15:3172–3203.

Fukunaga, K. (1990). Introduction to statistical pattern recognition. *Second ed., Academic Press*.

Fusiello, A., Trucco, E., Tommasini, T., and Roberto, V. (1999). Improving feature tracking with robust statistics. *Pattern Analysis and Applications*, 2:312–320.

Heikkilä, M., Pietikäinen, M., and Schmid, C. (2006). Description of interest regions with center-symmetric local binary patterns. In Madurai, I. L., editor, *5th Indian Conference on Computer Vision, Graphics and Image Processing*, volume 4338, pages 58–69.

Huang, Y., Wang, Y., and Tan, T. (2006). Combining statistics of geometrical and correlative features for 3d face recognition. In *17th British Machine Vision Conference*, pages 879–888.

Kailath, T. (1967). The divergence and bhattacharyya distance measures in signal selection. *IEEE Transactions on Communications Technology*, 15:52–60.

Lentmaier, M., Krach, B., and Robertson, P. (2008). Bayesian time delay estimation of gnss signals in dynamic multipath environments. *International Journal of Navigation and Observation*, vol. 2008.

Marais, J., Meurie, C., Attia, D., Ruichek, Y., and Flancquart, A. (2013). Toward accurate localization in guided transport: Combining gnss data and imaging information. *Transportation Research Part C Emerging Technologies*, 43:88–197.

Nanni, L., Brahnam, S., and Lumini, A. (2010a). A local approach based on a local binary patterns variant texture descriptor for classifying pain states. *Expert Syst. Appl*, 37(12):7888–7894.

Nanni, L., Lumini, A., and Brahnam, S. (2010b). Local binary patterns variants as texture descriptors for medical image analysis. *Artif. Intell. Med*, 49(2):117–125.

Ninga, J., Zhanga, L., and Wub, D. (2010). Interactive image segmentation by maximal similarity based region merging. *Pattern Recognition*, 43(2):445–456.

Nock, R. and Nielsen, F. (2004). Statistical region merging. *IEEE Transactions on Pattern Analysis Machine Intelligence*, 26:1452–1458.

Ojala, T., Pietikäinen, M., and Harwood, D. (1996). A comparative study of texture measures with classification based on feature distributions. *Pattern Recognit*, 29(1):51–59.

Ojansivu, V., , and Heikkila, J. (2008). Blur insensitive texture classification using local phase quantization. In *ICISP*, pages 236–243.

Stricker, M. and Orengo, M. (1995). Similarity of color images. In *SPIE Storage and Retrieval for Image and Video Databases*, volume 3, pages 381–392.

Swain, M. and Ballard, D. (2002). Color indexing. *International Journal of Computer Vision*, 7:11–32.

Tan, X. and Triggs, B. (2007). Enhanced local texture feature sets for face recognition under difficult lighting conditions. In LNCS, editor, *Analysis and Modelling of Faces and Gestures*, volume 4778, pages 168–182.

Unser, M. (1986). Sum and difference histograms for texture classification. *IEEE Trans. Pattern Anal. Mach. Intell . PAMI-8(1)*, pages 118–125.

Wang, J. and Gao, Y. (2007). High-sensitivity gps data classification based on signal degradation conditions. *IEEE Trans. Veh. Technol*, 56(2):566–574.

Zhang, B., Gao, Y., Zhao, S., and Liu, J. (2010). Local derivative pattern versus local binary pattern: face recognition with high-order local pattern descriptor. *IEEE Trans. Image Proces*, 19(2):533–544.